INTERNATIONAL JOURNAL FOR NUMERICAL METHODS IN FLUIDS
Int. J. Numer. Meth. Fluids 2008; **58**:781–802
Published online 17 March 2008 in Wiley InterScience (www.interscience.wiley.com). DOI: 10.1002/fld.1759

Numerical viscosity reduction in the resolution of the shallow water equations with turbulent term[‡]

J. Fe[1,3,*,†], L. Cueto-Felgueroso[4], F. Navarrina[1,3] and J. Puertas[2,3]

[1]*Grupo de Métodos Numéricos en Ingeniería, Universidad de A Coruña, Campus de Elviña, 15071 A Coruña, Spain*
[2]*Grupo de Ingeniería del Agua y del Medio Ambiente, Universidad de A Coruña, Campus de Elviña, 15071 A Coruña, Spain*
[3]*E.T.S. de Ingenieros de Caminos, Canales y Puertos, Universidad de A Coruña, Campus de Elviña, 15071 A Coruña, Spain*
[4]*Aerospace Computational Design Laboratory, Department of Aeronautics & Astronautics, Massachusetts Institute of Technology, 77 Massachusetts Ave, Cambridge, MA 02139, U.S.A.*

SUMMARY

A first-order finite volume model for the resolution of the 2D shallow water equations with turbulent term is presented. An upwind discretization of the equations that include the turbulent term is carried out. A method to reduce the excess of numerical viscosity (or diffusion) produced by the upwinding of the flux term is proposed. Two different discretizations of the turbulent term are compared, and results for uniform distributions of the viscosity are presented. Finally, two discretizations of the time derivative which are more efficient than Euler's are proposed and compared. Copyright © 2008 John Wiley & Sons, Ltd.

Received 30 October 2006; Revised 7 November 2007; Accepted 9 November 2007

KEY WORDS: finite volume; upwind; shallow water; numerical viscosity reduction; turbulent term; gradient mean values

[*] Correspondence to: J. Fe, E.T.S. de Ingenieros de Caminos, Canales y Puertos, Universidad de A Coruña, Campus de Elviña, 15071 A Coruña, Spain.

[†] E-mail: jfe@udc.es

[‡] This article was published online on 17 March 2008. An error was subsequently identified. This notice is included in the online and print versions to indicate that both have been corrected on 17 July 2008 (correction made here after initial online publication).

Contract/grant sponsor: Xunta de Galicia; contract/grant numbers: PGIDIT06TAM11801PR, PGIDIT05PXIC 118002PN
Contract/grant sponsor: Ministerio de Educación y Ciencia; contract/grant numbers: DPI2004-05156, DPI2006-15275, DPI2007-61214
Contract/grant sponsor: Universidad de A Coruña
Contract/grant sponsor: Fundación de la Ingeniería Civil de Galicia

1. INTRODUCTION

The behavior of a fluid in 3D may be described by the Navier–Stokes equations, which are a hyperbolic system of non-linear conservation laws. Their complexity has led to the development of the shallow water equations (SWE) based on some simplifying hypothesis, the most important of which is the hydrostatic pressure distribution [1]. The hydrostatic distribution can be assumed when the vertical length scale is much smaller than the horizontal one. This set of equations is suitable to describe the fluid behavior in domains with a small ratio of the depth (h) to the horizontal dimensions (L). It is not easy to establish an exact maximum ratio h/L to consider a flow to be shallow, but $\frac{1}{20}$ can be taken as a reference [1].

There are many flows in which the magnitude of the vertical velocity components is much smaller than the magnitude of the horizontal velocity components, at the space and time scales of interest for the resolution of a given problem (e.g. in coastal engineering or waste water treatment). In these cases, the depth-averaged form of the SWE (2D-SWE) provides a reasonable description of the velocity field.

The use of the 2D-SWE has increased dramatically during the last few decades and the application of finite element and finite volume discretizations to unstructured grids have become very popular. One of the most successful finite element schemes applied to the 2D-SWE is the Taylor–Galerkin algorithm proposed by Peraire *et al.* [2], which has been further developed by Quecedo and Pastor [3] who applied it to the drying–wetting problem. Ribeiro *et al.* [4] have formulated a discontinuity capturing operator to deal with fronts. Sheu and Fang [5] have proposed a generalized Taylor–Galerkin finite element method to obtain high resolution of discontinuous flows. Hauke [6] has applied the method to dam-break flood propagation and to irrigation flooding.

Most finite volume formulations for the 2D-SWE take advantage of the analogy between this system and the gas dynamics equations and have successfully been employed in the flow simulation. Alcrudo and García-Navarro [7] developed a Godunov-type MUSCL second-order scheme based on Roe's Riemann solver and a similar formulation was used by Chippada *et al.* [8]. Anastasiou and Chan [9] solved the 2D-SWE on unstructured meshes using a second-order Roe scheme whereas Zhao *et al.* [10] constructed their numerical flux using Osher's method. The finite volume formulation is probably the most widespread modelling strategy within the shallow water approximation [11] and it was the method used in our work.

The effects of turbulence are taken into account by 2D-SWE both through the frictional terms and the diffusion-like term that involves second derivatives. Frictional terms quantify the turbulence effects in the vertical, whereas the second derivatives term quantifies the turbulent losses produced by the horizontal mixing of momentum. This last term may not be significant in many practical problems when we only need an estimate of energy losses. In problems in which recirculation zones do not appear, thus exhibiting a 1D character, turbulent losses can be globally evaluated by an adequate choice of the friction coefficient. In tidal flows, the influence of turbulence in the mean velocity field can be almost negligible [12]. For these reasons, 2D-SWE are frequently used without considering the second derivatives (turbulent) term [7, 13–17]. However, as it will be shown in the cavity flow problem, this term may become necessary to properly describe flows in more general cases in which recirculation zones play a significant role.

An important point when working with the finite volume method (FVM) is to properly calculate the numerical flux at the cell edges. The upwinding of the flux term has proved to be a useful technique [7, 13, 15] with the drawback of producing a certain amount of numerical viscosity (or diffusion), which in some cases may be of similar magnitude to the turbulent viscosity. In order

DOI: 10.1002/fld

to reduce the numerical diffusion, some authors [7–9] use second-order methods. Other solutions are given by Cea *et al.* [12], who propose a hybrid algorithm (first order for the depth, second order for the velocity components), or Brocchini *et al.* [18], who use a second-order WAF method with local reduction to first-order near steep fronts. First-order schemes, however, such as the one described in the present work, are easier to implement and can give quite accurate results on the condition that the numerical viscosity is reduced.

The aim of the present paper is to show the influence of taking into account the turbulent term in the 2D-SWE, provided that the numerical viscosity produced by the discretization is reduced, while maintaining the simplicity of the first-order methods. In this paper, the equations that do not include the turbulent term and the model obtained from them will be denominated simplified, whereas the model considering this term will be called hydrodynamic.

The work is distributed as follows. In Section 2, the process to obtain the 2D-SWE from the 3D Navier–Stokes equations is summarized. In Section 3, the discretization of the simplified equations is described. Then the turbulent term is discretized (Section 4) and, in Section 5, the effect of its introduction into the equations and a method to diminish the numerical viscosity are shown. In Section 6, a comparison is made between the results obtained with two different discretizations of the turbulent term. Section 7 is devoted to describe and compare two alternative discretizations of the time derivative, which have proved to be much more efficient than Euler's.

2. 2D-SWE

To obtain the 2D-SWE, the Navier–Stokes equations are averaged in time, splitting velocity and pressure in the time average plus a fluctuation term. Owing to these fluctuating values, several new terms with stress dimensions appear, which are called Reynolds stresses. Boussinesq hypothesis relates these stresses to the derivatives of the time-averaged components of the velocity. By using this hypothesis, the derivatives of the Reynolds stresses become second derivative terms. If one accepts that the pressure distribution in the vertical direction is hydrostatic, the pressure gradient terms in the governing equations can be expressed in terms of the horizontal gradients of the water depth h. Finally, an integration over the depth is performed in which some of the second derivative terms give rise to the friction terms, whereas the rest of them constitute the so-called turbulent term. A detailed discussion can be found in [1, 19].

The 2D-SWE system in matrix form is expressed as

$$\frac{\partial \mathbf{U}}{\partial t}+\frac{\partial \mathbf{F_1}}{\partial x}+\frac{\partial \mathbf{F_2}}{\partial y}=\mathbf{G} \tag{1}$$

the vector of variables and the flux terms being

$$\mathbf{U}=\begin{pmatrix} h \\ hu \\ hv \end{pmatrix}, \quad \mathbf{F_1}=\begin{pmatrix} hu \\ hu^2+\frac{1}{2}gh^2 \\ huv \end{pmatrix}, \quad \mathbf{F_2}=\begin{pmatrix} hv \\ huv \\ hv^2+\frac{1}{2}gh^2 \end{pmatrix} \tag{2}$$

DOI: 10.1002/fld

and the source term being

$$\mathbf{G}=\begin{pmatrix} 0 \\ fvh+\dfrac{\tau_{s_x}}{\rho}+gh(S_{0x}-S_{fx})+S_{t1} \\ -fuh+\dfrac{\tau_{s_y}}{\rho}+gh(S_{0y}-S_{fy})+S_{t2} \end{pmatrix} \tag{3}$$

In the above expressions, h is the fluid depth; u and v are the horizontal velocity components; g is the gravity acceleration; f is the Coriolis coefficient and τ_{sx}, τ_{sy} are the wind stresses on the surface. The geometric slopes S_{0x}, S_{0y} are expressed in terms of H (see Figure 1)

$$S_{0x}=\frac{\partial H}{\partial x}, \quad S_{0y}=\frac{\partial H}{\partial y} \tag{4}$$

S_{fx}, S_{fy} are the friction slopes whose values, according to Manning's formula, are

$$S_{fx}=\frac{n^2 u\sqrt{u^2+v^2}}{R_h^{4/3}}, \quad S_{fy}=\frac{n^2 v\sqrt{u^2+v^2}}{R_h^{4/3}} \tag{5}$$

The hydraulic radius R_h is usually taken equal to h in the shallow water approach. Finally, S_t is the turbulent term. Owing to the simplifications made in the deduction process, several slightly different formulations for this term can be found in literature [2, 9, 20–22]. The expression used in the present work has been deduced in [19] and it has been compared [19, 22] with other expressions, achieving good results. The turbulent term, then, is expressed as

$$S_{t1}=\frac{\partial}{\partial x}\left(2v_t h\frac{\partial u}{\partial x}\right)+\frac{\partial}{\partial y}\left(v_t h\left[\frac{\partial v}{\partial x}+\frac{\partial u}{\partial y}\right]\right) \tag{6}$$

$$S_{t2}=\frac{\partial}{\partial x}\left(v_t h\left[\frac{\partial v}{\partial x}+\frac{\partial u}{\partial y}\right]\right)+\frac{\partial}{\partial y}\left(2v_t h\frac{\partial v}{\partial y}\right) \tag{7}$$

where the coefficient v_t is a variable called eddy viscosity.

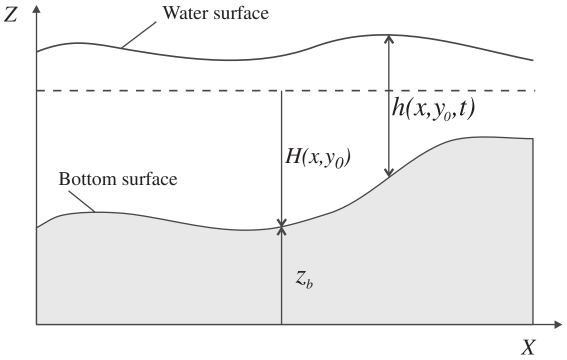

Figure 1. Representation of the variables H and h.

DOI: 10.1002/fld

The expressions (1)–(3) are the 2D-SWE in conservative form. When applied to small domains, the Coriolis term has little significance and it is usually neglected. The wind term can also be neglected when its influence is not relevant compared to the effect of the slope or the bottom friction, specifically in indoor laboratory channels. It is also common not to take into account the turbulent term [7, 13–17]. In this case, it is assumed that the turbulent energy losses are globally represented through the effect of S_f, provided that the friction coefficient is adequately chosen.

3. DISCRETIZATION OF THE SIMPLIFIED EQUATIONS

Now we are going to describe the discretization of the 2D-SWE without turbulent term to obtain the simplified model. Most of this section (particularly Sections 3.3 and 3.4) have been taken from the work of Bermúdez *et al.* [13], but we shall restate the equations and the solution method for the sake of completeness.

3.1. Construction of the finite volume mesh

The FVM proposed in this work is based on a triangular discretization of the domains so that the nodes of the triangular mesh are used as the nodes of the finite volume mesh (see Figure 2).

For each node I, the barycenters of the triangles with I as a common vertex and the mid-points of the edges that meet at I are taken. The boundary Γ_i of the cell C_i is obtained by joining these points. $\Gamma_{ij} = \overline{\mathrm{AMB}}$ represents the common part of Γ_i and Γ_j. The outward normal vector to Γ_{ij} is $\boldsymbol{\eta}_{ij}$. The norm of $\boldsymbol{\eta}_{ij}$, $\|\boldsymbol{\eta}_{ij}\|$, is the length of the edge and $\widetilde{\boldsymbol{\eta}}_{ij} = (\widetilde{\alpha}_{ij}, \widetilde{\beta}_{ij})^{\mathrm{T}}$ is the corresponding unit vector. The vector $\boldsymbol{\eta}_{ij}$ can have different magnitude and direction at $\overline{\mathrm{AM}}$ and at $\overline{\mathrm{MB}}$, thus

$$\boldsymbol{\eta}_{ij} = \begin{cases} \boldsymbol{\eta}_{ij}^{\mathrm{AM}} & \text{at } \overline{\mathrm{AM}} \\ \boldsymbol{\eta}_{ij}^{\mathrm{MB}} & \text{at } \overline{\mathrm{MB}} \end{cases} \tag{8}$$

The subcell T_{ij} is the union of triangles AMI and MBI.

3.2. Integration of the equations

Next the FVM is applied to the simplified form of the 2D-SWE, in which only the geometric and friction terms are considered. The expression of the source term (3) is then reduced to

$$\mathbf{G} = \begin{pmatrix} 0 \\ gh(S_{0x} - S_{fx}) \\ gh(S_{0y} - S_{fy}) \end{pmatrix} \tag{9}$$

Equation (1) can be expressed as

$$\frac{\partial \mathbf{U}}{\partial t} + \nabla \cdot \mathscr{F} = \mathbf{G}, \quad \mathscr{F}(\mathbf{U}) = (\mathbf{F_1}(\mathbf{U}), \mathbf{F_2}(\mathbf{U})) \tag{10}$$

DOI: 10.1002/fld

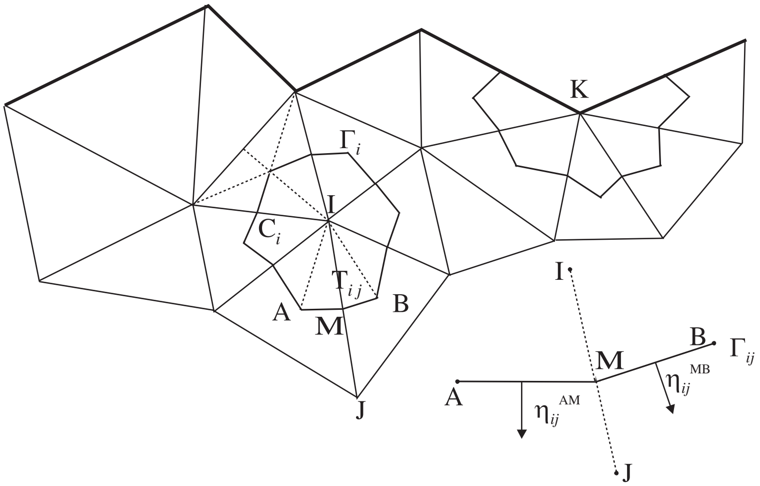

Figure 2. Finite volumes construction.

where ∇ is the operator $(\partial/\partial x, \partial/\partial y)$ and $\nabla\cdot\mathscr{F}$ is the divergence of $\mathscr{F}$. After the surface integral over the cell C_i is computed, we obtain

$$\iint_{C_i} \frac{\partial \mathbf{U}}{\partial t}\,\mathrm{d}A + \iint_{C_i} \nabla\cdot\mathscr{F}\,\mathrm{d}A = \iint_{C_i} \mathbf{G}\,\mathrm{d}A \tag{11}$$

The solution of (10) is now replaced by some values $\mathbf{U}_i^n$, constant within each cell C_i and at each time step t_n, ascribed to the cell center I. The time derivative is discretized by the forward Euler's method as

$$\left.\frac{\partial \mathbf{U}}{\partial t}\right|_{C_i,t_n} \approx \frac{\mathbf{U}_i^{n+1} - \mathbf{U}_i^n}{\triangle t} \tag{12}$$

whose value is constant over C_i and can be taken out of the corresponding integral in (11).

Now the Gauss theorem is applied to the flux term, dividing the boundary Γ_i into a sum of cell interfaces Γ_{ij}, $j \in \mathscr{K}_i$

$$\iint_{C_i} \nabla\cdot\mathscr{F}\,\mathrm{d}A = \sum_{j\in\mathscr{K}_i} \int_{\Gamma_{ij}} \mathscr{F}\cdot\tilde{\boldsymbol{\eta}}\,\mathrm{d}l \tag{13}$$

$\mathscr{K}_i$ being the set of neighboring nodes of I. We also split the integral source term in a sum of integrals over the subcells T_{ij}, $j \in \mathscr{K}_i$

$$\iint_{C_i} \mathbf{G}\,\mathrm{d}A = \sum_{j\in\mathscr{K}_i} \iint_{T_{ij}} \mathbf{G}\,\mathrm{d}A \tag{14}$$

3.3. Numerical flux definition

In order to evaluate the integral flux (13) at the cell boundary, the upwind Van Leer Q-scheme [23] is used, in the form proposed by Bermúdez *et al.* [13].

DOI: 10.1002/fld

The scalar product $\mathbf{Z}=\mathscr{F}\cdot\widetilde{\boldsymbol{\eta}}$, on $\Gamma_{ij}, j\in\mathscr{K}_i$ at $t=t_n$, is then approximated as

$$\boldsymbol{\phi}_{ij}^n=\frac{\mathbf{Z}(\mathbf{U}_i^n,\widetilde{\boldsymbol{\eta}}_{ij})+\mathbf{Z}(\mathbf{U}_j^n,\widetilde{\boldsymbol{\eta}}_{ij})}{2}-\frac{1}{2}|\mathbf{Q}(\mathbf{U}_Q^n,\widetilde{\boldsymbol{\eta}}_{ij})|(\mathbf{U}_j^n-\mathbf{U}_i^n) \tag{15}$$

In the above equation, $\mathbf{U}_i^n$ and $\mathbf{U}_j^n$ represent the variables values at I and J; $\mathbf{Q}$ is the jacobian matrix of $\mathbf{Z}$

$$\mathbf{Q}=\frac{\mathrm{d}\mathbf{Z}}{\mathrm{d}\mathbf{U}}=\widetilde{\alpha}\frac{\mathrm{d}\mathbf{F_1}}{\mathrm{d}\mathbf{U}}+\widetilde{\beta}\frac{\mathrm{d}\mathbf{F_2}}{\mathrm{d}\mathbf{U}} \tag{16}$$

$\widetilde{\alpha}$ and $\widetilde{\beta}$ being the components of $\widetilde{\boldsymbol{\eta}}_{ij}$ (the subscripts i, j are implied); $|\mathbf{Q}|$ is defined as

$$|\mathbf{Q}|=\mathbf{X}|\boldsymbol{\Lambda}|\mathbf{X}^{-1} \tag{17}$$

$|\boldsymbol{\Lambda}|$ being the diagonal matrix given by the absolute values of the eigenvalues of $\mathbf{Q}$ and $\mathbf{X}$ being the eigenvectors matrix of $\mathbf{Q}$. As the eigenvalues of $\mathbf{Q}$ are

$$\lambda_1=\widetilde{\alpha}u+\widetilde{\beta}v,\quad \lambda_2=\lambda_1+c,\quad \lambda_3=\lambda_1-c \tag{18}$$

c being the wave celerity $c=\sqrt{gh}$, the matrices $\mathbf{X}$ and $\mathbf{X}^{-1}$ take the form

$$\mathbf{X}=\begin{pmatrix}0 & 1 & 1\\ -\widetilde{\beta}c & u+\widetilde{\alpha}c & u-\widetilde{\alpha}c\\ \widetilde{\alpha}c & v+\widetilde{\beta}c & v-\widetilde{\beta}c\end{pmatrix},\quad \mathbf{X}^{-1}=\frac{1}{2c}\begin{pmatrix}2\widetilde{\beta}u-2\widetilde{\alpha}v & -2\widetilde{\beta} & 2\widetilde{\alpha}\\ c-\widetilde{\alpha}u-\widetilde{\beta}v & \widetilde{\alpha} & \widetilde{\beta}\\ c+\widetilde{\alpha}u+\widetilde{\beta}v & -\widetilde{\alpha} & -\widetilde{\beta}\end{pmatrix} \tag{19}$$

$|\mathbf{Q}|$ is evaluated at $\mathbf{U}_Q^n$, defined by

$$\mathbf{U}_Q^n=\frac{\mathbf{U}_i^n+\mathbf{U}_j^n}{2} \tag{20}$$

The second member of (14) is then expressed as

$$\sum_{j\in\mathscr{K}_i}\int_{\Gamma_{ij}}\mathscr{F}\cdot\widetilde{\boldsymbol{\eta}}\,\mathrm{d}l\approx\sum_{j\in\mathscr{K}_i}\|\boldsymbol{\eta}_{ij}\|\boldsymbol{\phi}_{ij}^n \tag{21}$$

3.4. Numerical source definition

Now the part of the source term that contains the geometrical slope is upwinded [13] by multiplying the contribution of each subcell by an upwinding factor. The friction slope has been treated in both ways, finding no substantial differences. Therefore, here it is calculated at the cell center. The numerical source, at each subcell T_{ij} and at each time step $t=t_n$, is then expressed as

$$\boldsymbol{\psi}_{ij}^n=(\mathbf{I}-|\mathbf{Q}|\mathbf{Q}^{-1})\widehat{\mathbf{G}}_\mathbf{0}+\widehat{\mathbf{G}}_\mathbf{f} \tag{22}$$

DOI: 10.1002/fld

where the numerical geometric slope $\widehat{\mathbf{G}}_{\mathbf{0}}$ and the numerical friction slope $\widehat{\mathbf{G}}_{\mathbf{f}}$ are

$$\widehat{\mathbf{G}}_{\mathbf{0}}=\begin{pmatrix} 0 \\ g\dfrac{h_i^n+h_j^n}{2}\dfrac{H_j-H_i}{d_{ij}}\widetilde{\alpha} \\ g\dfrac{h_i^n+h_j^n}{2}\dfrac{H_j-H_i}{d_{ij}}\widetilde{\beta} \end{pmatrix}, \quad \widehat{\mathbf{G}}_{\mathbf{f}}=\begin{pmatrix} 0 \\ gh_i^n(-S_{fx})_i^n \\ gh_i^n(-S_{fy})_i^n \end{pmatrix} \tag{23}$$

d_{ij} being the normal distance from I to Γ_{ij} that has different values at the two subcell triangles AMI and MBI. The second member of (14) becomes

$$\sum_{j\in\mathscr{K}_i}\iint_{T_{ij}}\mathbf{G}\,\mathrm{d}A\approx\sum_{j\in\mathscr{K}_i}A_{ij}\boldsymbol{\psi}_{ij}^n \tag{24}$$

A_{ij} being the area of each subcell.

3.5. Time step

To estimate the time step we have used the expression proposed by Brufau and García-Navarro [16]

$$\triangle t\leqslant 0.5\cdot\min\left(\frac{D_{ij}}{(\sqrt{u^2+v^2}+c)_{ij}}\right) \tag{25}$$

where D_{ij} are the distances between each node I and its neighboring nodes and 0.5 is a coefficient to ensure stability.

3.6. Algorithm

Using the above described method, a discretization of Equation (11) has been obtained, which takes the form

$$\frac{\mathbf{U}_i^{n+1}-\mathbf{U}_i^n}{\triangle t}A_i+\sum_{j\in\mathscr{K}_i}\|\boldsymbol{\eta}_{ij}\|\boldsymbol{\phi}_{ij}^n=\sum_{j\in\mathscr{K}_i}A_{ij}\boldsymbol{\psi}_{ij}^n \tag{26}$$

then

$$\mathbf{U}_i^{n+1}=\mathbf{U}_i^n+\frac{\triangle t}{A_i}\left(\sum_{j\in\mathscr{K}_i}A_{ij}\boldsymbol{\psi}_{ij}^n-\sum_{j\in\mathscr{K}_i}\|\boldsymbol{\eta}_{ij}\|\boldsymbol{\phi}_{ij}^n\right) \tag{27}$$

Equation (27) provides a time explicit method to calculate the variables value at every node I and at every time step from the previous time step values at node I and its neighboring nodes.

4. THE TURBULENT SOURCE TERM

In Sections 1 and 2, we emphasized that when using the 2D-SWE, it is common not to take into account the term that contains the second derivatives of u and v. This assumption works well in many cases such as in practical problems when we only need to estimate energy losses or

DOI: 10.1002/fld

in problems without recirculation zones. However, the consideration of the spatial variation of u and v may prove to be necessary for the description of flows in which recirculation zones play a significant role.

In this section, the addends S_{t1} and S_{t2} of the source term given by (6) and (7) will be considered. Their surface integral over each cell C_i can be expressed as

$$\left\{\begin{matrix} 0 \\ \displaystyle\iint_{\mathrm{C}_i} S_{t1}\,\mathrm{d}A \\ \displaystyle\iint_{\mathrm{C}_i} S_{t2}\,\mathrm{d}A \end{matrix}\right\} = \left\{\begin{matrix} 0 \\ \displaystyle\iint_{\mathrm{C}_i} \nabla\cdot\left(2v_t h\frac{\partial u}{\partial x}, v_t h\left[\frac{\partial v}{\partial x}+\frac{\partial u}{\partial y}\right]\right)\mathrm{d}A \\ \displaystyle\iint_{\mathrm{C}_i} \nabla\cdot\left(v_t h\left[\frac{\partial v}{\partial x}+\frac{\partial u}{\partial y}\right], 2v_t h\frac{\partial v}{\partial y}\right)\mathrm{d}A \end{matrix}\right\} \tag{28}$$

As already done in Section 3.2, the Gauss theorem is applied in every cell, splitting the line integral over Γ_i in a sum of integrals over the cell sides Γ_{ij}, $j\in\mathscr{K}_i$. It results in

$$\left\{\begin{matrix} 0 \\ \displaystyle\sum_{j\in\mathscr{K}_i}\int_{\Gamma_{ij}} \left(2v_t h\frac{\partial u}{\partial x}, v_t h\left[\frac{\partial v}{\partial x}+\frac{\partial u}{\partial y}\right]\right)\cdot(\widetilde{\alpha},\widetilde{\beta})\,\mathrm{d}l \\ \displaystyle\sum_{j\in\mathscr{K}_i}\int_{\Gamma_{ij}} \left(v_t h\left[\frac{\partial v}{\partial x}+\frac{\partial u}{\partial y}\right], 2v_t h\frac{\partial v}{\partial y}\right)\cdot(\widetilde{\alpha},\widetilde{\beta})\,\mathrm{d}l \end{matrix}\right\} \tag{29}$$

In expression (29) we need to estimate the partial derivatives values at every cell side. Two methods have been used: (a) from the derivatives of u and v with respect to η (normal direction to Γ) and (b) from the mean values of ∇u and ∇v at the adjacent cells.

4.1. From the directional derivatives

Let η, τ be two normal directions and $\widetilde{\boldsymbol{\eta}}, \widetilde{\boldsymbol{\tau}}$ the corresponding unit vectors. We have

$$\frac{\partial u}{\partial\eta} = \nabla u\cdot\widetilde{\boldsymbol{\eta}} = \frac{\partial u}{\partial x}\widetilde{\eta}_1 + \frac{\partial u}{\partial y}\widetilde{\eta}_2 \tag{30}$$

$$\frac{\partial u}{\partial\tau} = \nabla u\cdot\widetilde{\boldsymbol{\tau}} = \frac{\partial u}{\partial x}\widetilde{\tau}_1 + \frac{\partial u}{\partial y}\widetilde{\tau}_2 \tag{31}$$

or, in matrix form,

$$\left\{\begin{matrix} \dfrac{\partial u}{\partial\eta} \\ \dfrac{\partial u}{\partial\tau} \end{matrix}\right\} = \begin{pmatrix} \widetilde{\eta}_1 & \widetilde{\eta}_2 \\ \widetilde{\tau}_1 & \widetilde{\tau}_2 \end{pmatrix} \left\{\begin{matrix} \dfrac{\partial u}{\partial x} \\ \dfrac{\partial u}{\partial y} \end{matrix}\right\} \tag{32}$$

DOI: 10.1002/fld

As $\tilde{\boldsymbol{\tau}}$ is normal to $\tilde{\boldsymbol{\eta}}$, calculating the inverse matrix

$$\left\{\begin{matrix}\dfrac{\partial u}{\partial x}\\[2ex] \dfrac{\partial u}{\partial y}\end{matrix}\right\}=\begin{pmatrix}\eta_1 & -\eta_2\\ \eta_2 & \eta_1\end{pmatrix}\left\{\begin{matrix}\dfrac{\partial u}{\partial \eta}\\[2ex] \dfrac{\partial u}{\partial \tau}\end{matrix}\right\} \tag{33}$$

Now, let τ be the direction of the cell side and η the normal to it, with $(\tilde{\eta}_1,\tilde{\eta}_2)^{\mathrm{T}}=(\tilde{\alpha},\tilde{\beta})^{\mathrm{T}}$ as unit vector. The velocity component u is assumed to be constant within C_i. Then, if the value of u does not change along the side, its derivative with respect to τ is zero and we obtain

$$\left\{\begin{matrix}\dfrac{\partial u}{\partial x}\\[2ex] \dfrac{\partial u}{\partial y}\end{matrix}\right\}=\begin{pmatrix}\tilde{\alpha} & -\tilde{\beta}\\ \tilde{\beta} & \tilde{\alpha}\end{pmatrix}\left\{\begin{matrix}\dfrac{\partial u}{\partial \eta}\\[2ex] 0\end{matrix}\right\}=\left\{\begin{matrix}\tilde{\alpha}\dfrac{\partial u}{\partial \eta}\\[2ex] \tilde{\beta}\dfrac{\partial u}{\partial \eta}\end{matrix}\right\} \tag{34}$$

likewise

$$\left\{\begin{matrix}\dfrac{\partial v}{\partial x}\\[2ex] \dfrac{\partial v}{\partial y}\end{matrix}\right\}=\left\{\begin{matrix}\tilde{\alpha}\dfrac{\partial v}{\partial \eta}\\[2ex] \tilde{\beta}\dfrac{\partial v}{\partial \eta}\end{matrix}\right\} \tag{35}$$

These directional derivatives can be discretized as

$$\frac{\partial u}{\partial \eta}=\frac{u_j-u_i}{2d_{ij}} \tag{36}$$

$$\frac{\partial v}{\partial \eta}=\frac{v_j-v_i}{2d_{ij}} \tag{37}$$

$2d_{ij}$ being the length of the projection of $\overline{\mathrm{IJ}}$ over η.

In Section 3.4, a numerical source term has been defined. Multiplied by each subcell area, it approximates the surface integral of the geometric and friction source terms (24). Now a line integral is calculated; then the discretized integral of the turbulent source term corresponding to a unit side length at $t=t_n$ takes the form

$$\widehat{\mathbf{G}}_{\mathbf{t}}=\left\{\begin{matrix}0\\[1ex] \dfrac{v_{ti}+v_{tj}}{2}\dfrac{h_i^n+h_j^n}{2}\left[2\dfrac{u_j^n-u_i^n}{2d_{ij}}\tilde{\alpha}^2+\dfrac{v_j^n-v_i^n}{2d_{ij}}\tilde{\alpha}\tilde{\beta}+\dfrac{u_j^n-u_i^n}{2d_{ij}}\tilde{\beta}^2\right]\\[3ex] \dfrac{v_{ti}+v_{tj}}{2}\dfrac{h_i^n+h_j^n}{2}\left[\dfrac{v_j^n-v_i^n}{2d_{ij}}\tilde{\alpha}^2+\dfrac{u_j^n-u_i^n}{2d_{ij}}\tilde{\alpha}\tilde{\beta}+2\dfrac{v_j^n-v_i^n}{2d_{ij}}\tilde{\beta}^2\right]\end{matrix}\right\} \tag{38}$$

In this expression, the viscosity has no time index since it is assumed that its values can vary at every node, but they are not time dependent. Obviously this is an assumption, since eddy viscosity could also vary in time. However, taking into account this effect is beyond the scope of this work since it would require the use of a turbulence model. This issue will be addressed in forthcoming papers.

4.2. From the gradient mean values

Here the partial derivatives of u and v at Γ_{ij} are obtained as the components of their gradient. To approximate the gradient of a scalar magnitude m at Γ_{ij}, the mean value of its gradients at cells C_i and C_j is used. The gradient of m within C_i is estimated as

$$(\overline{\nabla m})_{\mathrm{C}_i} = \frac{1}{A_i}\iint_{\mathrm{C}_i} \nabla m \,\mathrm{d}A \tag{39}$$

and the surface integral of ∇m over C_i is calculated as [19]

$$\iint_{\mathrm{C}_i} \nabla m \,\mathrm{d}A = \int_{\Gamma_i} m\mathbf{n}\,\mathrm{d}l \tag{40}$$

$\mathbf{n}$ being the unit vector normal to Γ_i. Since

$$\mathbf{n} = \tilde{\boldsymbol{\eta}} = \tilde{\alpha}\mathbf{i} + \tilde{\beta}\mathbf{j} \tag{41}$$

and

$$(\overline{\nabla m})_{\mathrm{C}_i} = \left(\overline{\frac{\partial m}{\partial x}}\right)_{\mathrm{C}_i}\mathbf{i} + \left(\overline{\frac{\partial m}{\partial y}}\right)_{\mathrm{C}_i}\mathbf{j} \tag{42}$$

where $\mathbf{i}$ is the x-axis unit vector and i is the cell index, the average values of the partial derivatives of m within C_i become

$$\left(\overline{\frac{\partial m}{\partial x}}\right)_{\mathrm{C}_i} = \frac{1}{A_i}\int_{\Gamma_i} m\tilde{\alpha}\,\mathrm{d}l = \frac{1}{A_i}\sum_{j\in\mathscr{K}_i}\int_{\Gamma_{ij}} m\tilde{\alpha}\,\mathrm{d}l \tag{43}$$

$$\left(\overline{\frac{\partial m}{\partial y}}\right)_{\mathrm{C}_i} = \frac{1}{A_i}\int_{\Gamma_i} m\tilde{\beta}\,\mathrm{d}l = \frac{1}{A_i}\sum_{j\in\mathscr{K}_i}\int_{\Gamma_{ij}} m\tilde{\beta}\,\mathrm{d}l \tag{44}$$

Then the process is summarized as follows. First, the values of u, v at Γ_{ij} are estimated as their mean value at nodes I and J. Then the partial derivatives of u and v within each cell C_i are obtained from the estimated values of u, v at Γ_{ij} by

$$\left(\overline{\frac{\partial u}{\partial x}}\right)_{\mathrm{C}_i} = \frac{1}{A_i}\sum_{j\in\mathscr{K}_i}\frac{u_i+u_j}{2}\tilde{\alpha}\|\boldsymbol{\eta}_{ij}\|, \quad \left(\overline{\frac{\partial v}{\partial x}}\right)_{\mathrm{C}_i} = \frac{1}{A_i}\sum_{j\in\mathscr{K}_i}\frac{v_i+v_j}{2}\tilde{\alpha}\|\boldsymbol{\eta}_{ij}\| \tag{45}$$

$$\left(\overline{\frac{\partial u}{\partial y}}\right)_{\mathrm{C}_i} = \frac{1}{A_i}\sum_{j\in\mathscr{K}_i}\frac{u_i+u_j}{2}\tilde{\beta}\|\boldsymbol{\eta}_{ij}\|, \quad \left(\overline{\frac{\partial v}{\partial y}}\right)_{\mathrm{C}_i} = \frac{1}{A_i}\sum_{j\in\mathscr{K}_i}\frac{v_i+v_j}{2}\tilde{\beta}\|\boldsymbol{\eta}_{ij}\| \tag{46}$$

DOI: 10.1002/fld

and we can finally obtain the partial derivatives at Γ_{ij} as the mean value of the derivatives at C_i and C_j. By expressing the values of the partial derivatives of u and v within C_i at time $t=t_n$ as

$$u^n_{xi}=\left(\overline{\frac{\partial u}{\partial x}}\right)_{\mathrm{C}_i,t_n},\quad v^n_{xi}=\left(\overline{\frac{\partial v}{\partial x}}\right)_{\mathrm{C}_i,t_n} \tag{47}$$

$$u^n_{yi}=\left(\overline{\frac{\partial u}{\partial y}}\right)_{\mathrm{C}_i,t_n},\quad v^n_{yi}=\left(\overline{\frac{\partial v}{\partial y}}\right)_{\mathrm{C}_i,t_n} \tag{48}$$

the discretized integral of the turbulent source term at Γ_{ij} and at $t=t_n$ is

$$\widehat{\mathbf{G}}_{\mathbf{t}}=\left\{\begin{matrix} 0 \\ \dfrac{v_{ti}+v_{tj}}{2}\dfrac{h^n_i+h^n_j}{2}\left(2\dfrac{u^n_{xi}+u^n_{xj}}{2}\tilde{\alpha}+\dfrac{v^n_{xi}+v^n_{xj}}{2}\tilde{\beta}+\dfrac{u^n_{yi}+u^n_{yj}}{2}\tilde{\beta}\right) \\ \dfrac{v_{ti}+v_{tj}}{2}\dfrac{h^n_i+h^n_j}{2}\left(\dfrac{v^n_{xi}+v^n_{xj}}{2}\tilde{\alpha}+\dfrac{u^n_{yi}+u^n_{yj}}{2}\tilde{\alpha}+2\dfrac{v^n_{yi}+v^n_{yj}}{2}\tilde{\beta}\right) \end{matrix}\right\} \tag{49}$$

where again it is assumed that the values of v_t can vary at every node, but they are not time dependent.

4.3. The numerical turbulent source

Finally, the surface integral of the turbulent term (28) is approximated by an expression similar to (24)

$$\sum_{j\in\mathscr{K}_i}\iint_{T_{ij}}\mathbf{G}\,\mathrm{d}A\approx\sum_{j\in\mathscr{K}_i}\|\boldsymbol{\eta}_{ij}\|\boldsymbol{\psi}^n_{vij} \tag{50}$$

where $\boldsymbol{\psi}^n_{vij}$ is the numerical turbulent source that takes either the form (38) or (49). Then including the turbulent term, algorithm (27) changes to

$$\mathbf{U}^{n+1}_i=\mathbf{U}^n_i+\frac{\Delta t}{A_i}\left(\sum_{j\in\mathscr{K}_i}(A_{ij}\boldsymbol{\psi}^n_{ij}+\|\boldsymbol{\eta}_{ij}\|\boldsymbol{\psi}^n_{vij})-\sum_{j\in\mathscr{K}_i}\|\boldsymbol{\eta}_{ij}\|\boldsymbol{\phi}^n_{ij}\right) \tag{51}$$

5. VALIDATION OF THE HYDRODYNAMIC MODEL FOR UNIFORM VALUES OF THE VISCOSITY

The discretization of the turbulent term (Sections 4.1 and 4.2) has been done to admit different viscosity values at every node, which is usually the case in real turbulent flows. However, we are going to test the model for uniform values of the viscosity. Using a non-uniform viscosity throughout the domain would require to obtain the viscosity values from a turbulence model, which is beyond the scope of the present work. In any case, it would not pose any numerical problem because we would only need to make an average of the viscosity values—see expressions (38) and (49)—at every two nodes to obtain the value at the edge between them.

DOI: 10.1002/fld

5.1. Cavity flow: first results

To check the effectiveness of introducing the turbulent term in the 2D-SWE, as well as to compare two discretizations of it (that will be described in Section 6), the cavity flow problem has been chosen. It is a classical benchmark for the 2D Navier–Stokes equations with a maximum Reynolds number of 10 000, over which value the steady solution becomes unstable [21]. In the cavity flow, the form of the streamlines, the u-velocity at the central section and the position of the circulation center, depend completely on the imposed value of the viscosity.

This test is not common in the shallow water literature and experimental results have not been found as it might be expected. However, there are many numerical results and comparisons between them [21, 24–27].

From the 3D form of the Navier–Stokes equations 2D-SWE are obtained through a process summarized in Section 2. They are different from the 2D Navier–Stokes equations. The latter do not take into account the third dimension in space but only the velocities and pressures of a theoretical planar flow, whereas 2D-SWE consider the third dimension by means of the variable depth and the pressure is expressed as a function of the depth. However, as it will be shown, both systems produce very similar results with uniform viscosity values and only slight differences must be expected between the corresponding solutions to these problems. For this reason, the analysis of these test results may be very useful to assess the ability of the proposed numerical scheme to capture fine viscous features of the flow.

The problem consists of obtaining the velocity field in a square domain of $1\times 1\,\mathrm{m}^2$. A regular mesh of 81×81 nodes is employed (its central part is represented in Figure 3). The boundary conditions of Dirichlet type are: $u=1, v=0$ at the upper side; $u=v=0$ (no-slip condition) at the other three. The variables used are h, hu and hv; thus the actual imposed conditions at the upper side are $h=1, hu=1, hv=0$.

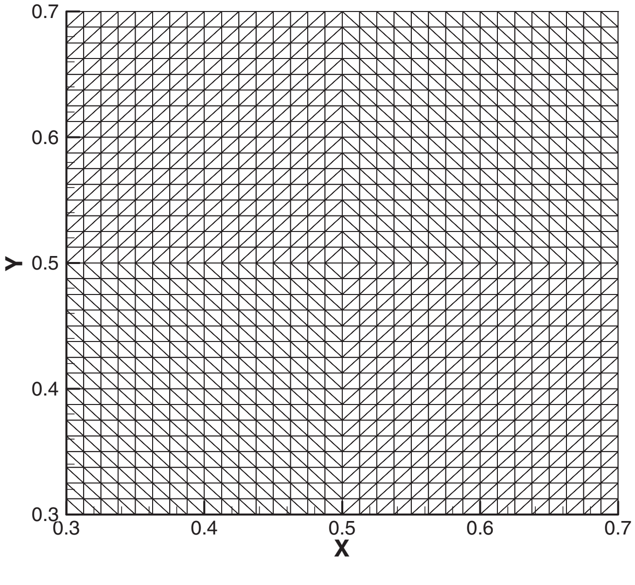

Figure 3. Cavity flow: mesh.

Results must depend on the Reynolds number used. Taking the values $V=1$ and $L=1$ for the velocity and length scales, the resulting Re values are

$$Re=\frac{VL}{v}=\frac{1}{v} \tag{52}$$

which allows us to simulate different Reynolds numbers by varying the viscosity value.

In the first place, a case without viscosity was examined. Then two other cases with a v value of 0.0025 and 0.01 m^2/s, corresponding to Reynolds numbers of 400 and 100, respectively, were solved. The streamlines in the three cases can be seen in Figure 4. Figure 5 shows the comparison of the velocity components u, at $x=0.5\,\mathrm{m}$, for the three cases. As it can be observed, the resulting difference between the three cases is much smaller than the expected, and the reason must be found in the high numerical viscosity (or diffusion) inherent in first-order methods, which does

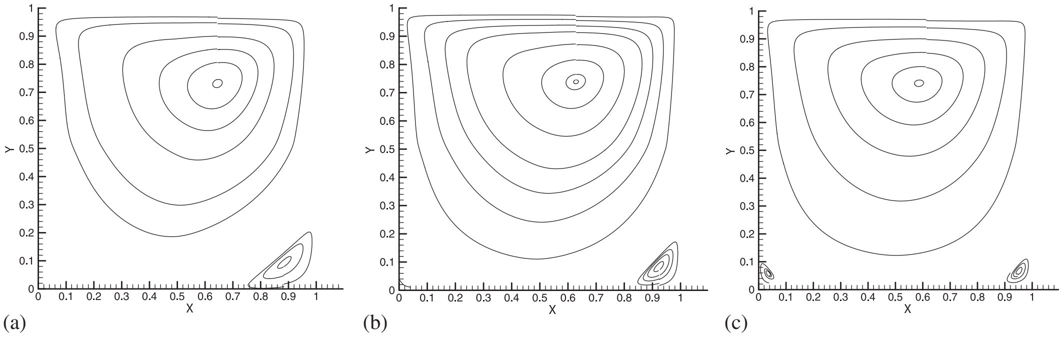

Figure 4. Streamlines: (a) $v=0$; (b) $v=0.025$; and (c) $v=0.01$.

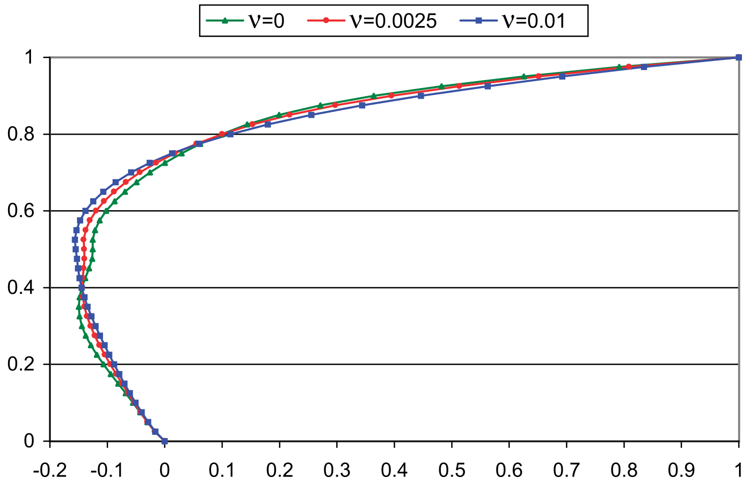

Figure 5. u velocities at $x=0.5$ for different viscosities.

not allow us to appreciate the effect of a viscosity value difference of 0.01. This numerical viscosity is known to depend on the mesh size [19] and, even with a reasonably fine mesh such as the one used here, its effects are unacceptable.

5.2. Reduction of the numerical viscosity

In Section 3.3, the Q-scheme of Van Leer was used to calculate the flux values at every cell boundary. This approximation can be interpreted stating that the flux at a cell boundary is the sum of a centered average of the fluxes on both sides of the boundary plus an upwinding term. This term stabilizes the system at the expense of introducing a certain amount of numerical diffusion. Therefore, in order to make the model less diffusive, the upwinding term needs to be reduced as much as possible, while the stability is kept. This can be achieved [28] by using an upwinding coefficient c_d, so that expression (15) becomes

$$\boldsymbol{\phi}_{ij}^n = \frac{\mathbf{Z}(\mathbf{U}_i^n, \tilde{\boldsymbol{\eta}}_{ij}) + \mathbf{Z}(\mathbf{U}_j^n, \tilde{\boldsymbol{\eta}}_{ij})}{2} - c_d \frac{1}{2} |\mathbf{Q}(\mathbf{U}_Q^n, \tilde{\boldsymbol{\eta}}_{ij})| (\mathbf{U}_j^n - \mathbf{U}_i^n), \quad 0 \leqslant c_d \leqslant 1 \tag{53}$$

The suitable value of this coefficient is the smallest that can provide stable calculations. If $c_d = 0$, the scheme is a centered one. If $c_d = 1$, there is no upwinding term reduction. Lin *et al.* [29] have successfully used a c_d value of 0.1 in acoustic computations. In the large eddy simulation model described by Bui [28], smaller values (0.03–0.05) were needed to obtain good results. Diminishing the c_d value increases the computational cost because the minimum value of this coefficient necessary for stability decreases with the mesh size [28]; that is to say, to diminish the c_d acceptable values, finer grids have to be used.

After a trial-and-error process, the most appropriate value was found to be $c_d = 0.03$, with the 81×81 nodes mesh. In this case, the streamlines corresponding to four viscosity values (Figure 6) and the velocities at the central section corresponding to three viscosity values (Figure 7) are shown.

5.3. Comparison of the positions of the centers

To test the effectiveness of the described method to reduce the numerical viscosity, a comparison is made (Table I) between the main eddy center coordinates obtained with the model and some references [21, 24, 26]. The main eddy centers are plotted in Figure 8. Several conclusions can be drawn as follows:

- For $Re = 100$, the results are in an intermediate position among the references.
- For $Re = 400$, the x-coordinate of the eddy center is displaced slightly rightwards with respect to the references. The y-coordinate is in an intermediate position.
- For $Re = 1000$, the y-coordinate of the eddy center is displaced slightly over the other results. The x-coordinate is in an intermediate position.
- For $Re = 10\,000$, the eddy center is slightly over and on the right of the reference result.

We can see that the results match very well with the reference values for low Reynolds numbers. However, as the Reynolds number increases, the main eddy center moves slightly upwards and rightwards with respect to the reference results. On the other hand, we observe in Figure 6 that the main eddy center moves upwards and rightwards with a rise of the viscosity value. Also, Figure 9 represents the evolution of the main eddy center coordinates, for seven Reynolds number

DOI: 10.1002/fld

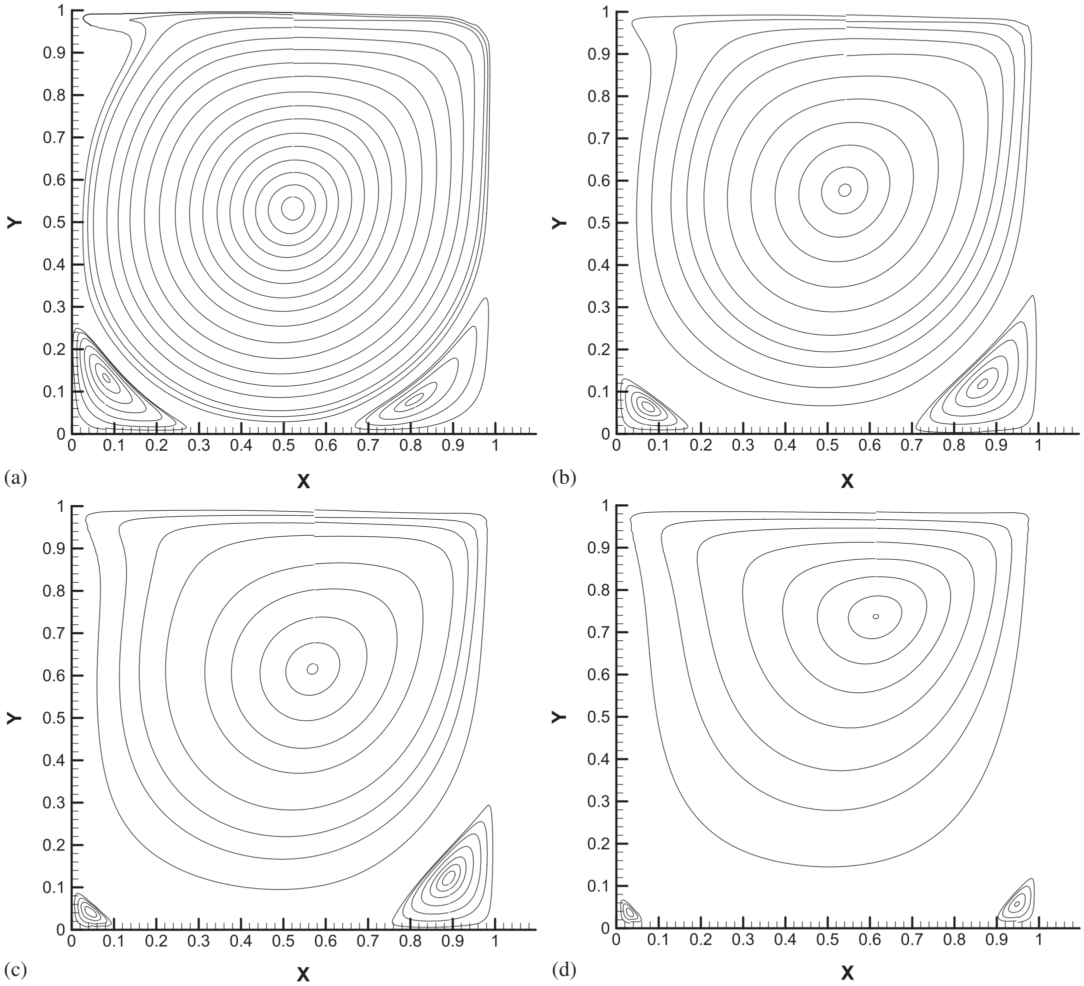

Figure 6. $c_d = 0.03$. Streamlines (from left to right and top to bottom): (a) $\nu = 0.0001$ ($Re = 10\,000$); (b) $\nu = 0.001$ ($Re = 1000$); (c) $\nu = 0.0025$ ($Re = 400$); and (d) $\nu = 0.01$ ($Re = 100$).

values from 100 to 10 000. It can be seen that both coordinates increase as the Reynolds number decreases, which corresponds to an increase in the viscosity value. These last results have been obtained using a very fine 257×257 mesh [27].

The described phenomenon explains the slight change in the relative position of the main eddy center with respect to the references: the part of numerical viscosity that the upwinding coefficient is not able to eliminate becomes more important when the imposed viscosity value decreases.

It can be concluded that the introduction of the turbulent term in the 2D-SWE improves their ability to represent 2D flows with recirculation zones. It is also noted that the numerical viscosity introduced by the upwinding, although reduced by the use of c_d, has a fixed value which is more

DOI: 10.1002/fld

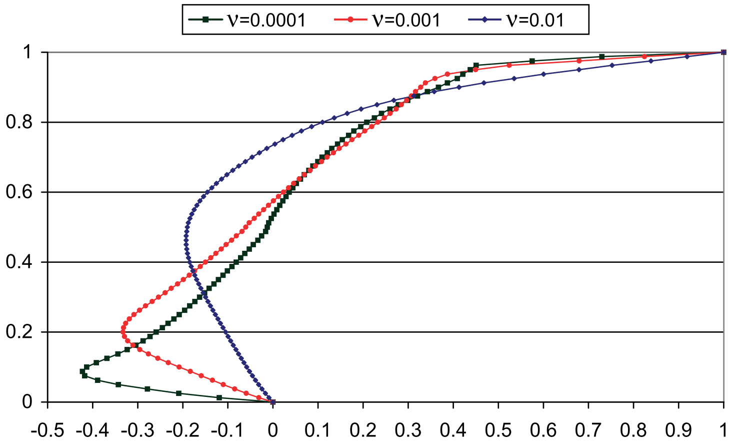

Figure 7. $c_d = 0.03$. u velocities at $x = 0.5$ for different viscosities.

Table I. Coordinates of the main eddy center.

Reynolds number	References	x_c	y_c
	Burggraff [24]	0.62	0.74
$Re = 100$	Donea and Huerta [26]	0.62	0.74
($v = 0.01$)	Vellando *et al.* [21]	0.610	0.735
	Present	0.615	0.737
	Burggraff [24]	0.560	0.620
$Re = 400$	Donea and Huerta [26]	0.568	0.606
($v = 0.0025$)	Present	0.569	0.615
	Donea and Huerta [26]	0.540	0.573
$Re = 1000$	Vellando *et al.* [21]	0.545	0.565
($v = 0.001$)	Present	0.541	0.577
$Re = 10000$	Vellando *et al.* [21]	0.520	0.530
($v = 0.0001$)	Present	0.523	0.533

significant when the imposed v value decreases; that is to say, the behavior of the model is more diffusive for lesser values of the viscosity.

6. COMPARISON OF THE DISCRETIZATIONS OF THE TURBULENT TERM

We have seen the influence of including the turbulent term in the 2D-SWE on representing flows accurately with uniform distributions of the viscosity. Now we shall take advantage of this fact to compare two discretizations of the turbulent term.

The first discretization uses the directional derivatives and it has been described in Section 4.1. The second one is obtained from the gradient mean values and it has been described in Section 4.2. The streamlines obtained with both discretizations for a Reynolds number of 1000 are similar in

DOI: 10.1002/fld

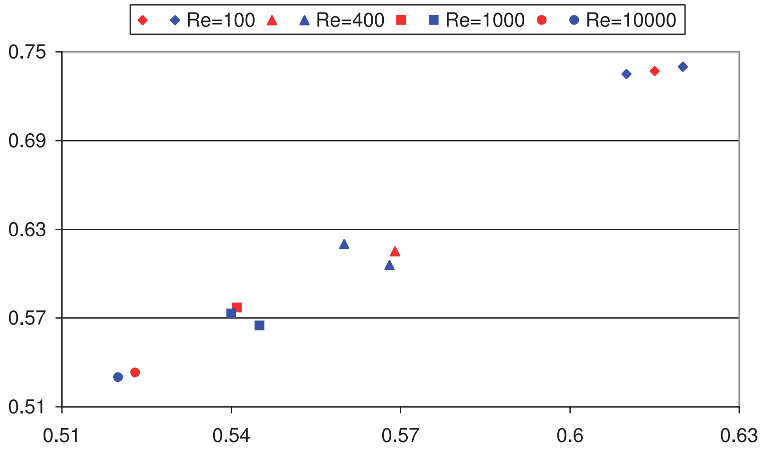

Figure 8. Main eddy center positions (results in red; references in blue).

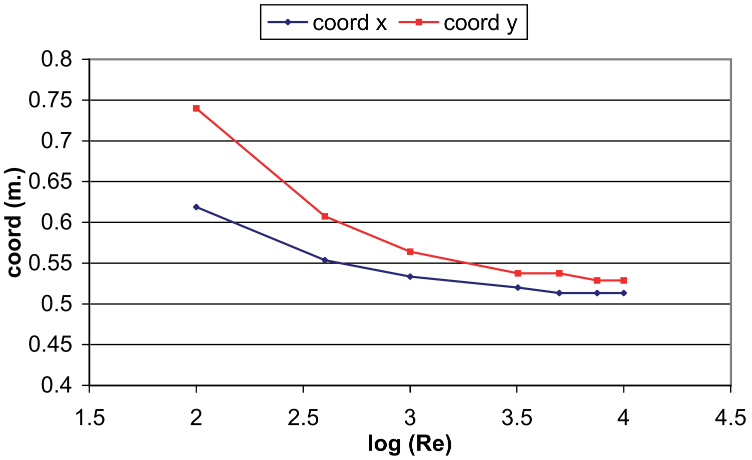

Figure 9. Main eddy center. Evolution of the position with *Re*.

aspect; the second one has been represented in Figure 6(b). Yet, there is a remarkable difference between the center coordinates, which in the second case are smaller and closer to the reference values (Table I) than in the first one. These values are:

- *Directional derivatives*: $x_c = 0.556$, $y_c = 0.597$.
- *Gradient mean values*: $x_c = 0.541$, $y_c = 0.577$.

Moreover, the horizontal velocities at the central section are compared in Figure 10, taking the results of [26] as a reference. It may be seen that the second method matches the reference values much better than the first one, producing a sharper and more adequate profile. We can conclude that the turbulent term discretization that uses the gradient mean values has yielded more accurate and less diffusive results.

DOI: 10.1002/fld

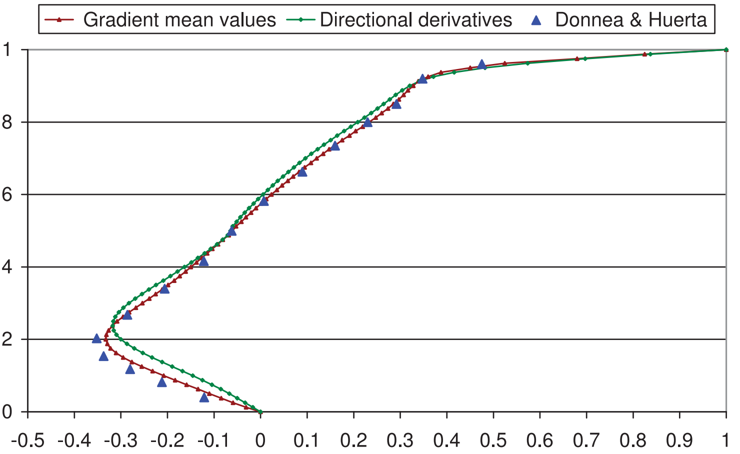

Figure 10. $\nu=0.001$. u velocities at $x=0.5$ for different discretizations.

7. ALTERNATIVE DISCRETIZATIONS OF THE TIME DERIVATIVE

The time step for the simplified model is calculated from expression (25), usually posing no stability problems. It has been observed, however, that the numerical viscosity reduction produces a drastic decrease in the acceptable time step, thus making the process very expensive from a computational point of view. To solve this problem, two alternative time derivative discretizations have been implemented and compared: the fourth-order predictor–corrector Adams–Moulton method and the fourth-order Runge–Kutta method.

Both discretizations have proved to be much more efficient than the forward Euler method; the Adams–Moulton method is almost seven times faster than Euler's and the Runge–Kutta method is almost ten times faster, in one of the tests carried out. We shall describe both methods and compare them for two viscosity values.

In the fourth-order predictor–corrector Adams–Moulton, the predictor formula [30] is

$$\mathbf{U}^{n+1}=\mathbf{U}_n+\frac{\triangle t}{24}(55\boldsymbol{\varphi}_n-59\boldsymbol{\varphi}_{n-1}+37\boldsymbol{\varphi}_{n-2}-9\boldsymbol{\varphi}_{n-3}) \tag{54}$$

and the corrector

$$\mathbf{U}^{n+1}=\mathbf{U}_n+\frac{\triangle t}{24}(9\boldsymbol{\varphi}_{n+1}+19\boldsymbol{\varphi}_n-5\boldsymbol{\varphi}_{n-1}+\boldsymbol{\varphi}_{n-2}) \tag{55}$$

The fourth-order Runge–Kutta formula is [30]

$$\mathbf{U}^{n+1}=\mathbf{U}^n+\triangle t\boldsymbol{\Phi}(t^n,\mathbf{U}^n) \tag{56}$$

where

$$\boldsymbol{\Phi}(t^n,\mathbf{U}^n)=\frac{\mathbf{k}_0+2\mathbf{k}_1+2\mathbf{k}_2+\mathbf{k}_3}{6} \tag{57}$$

with

$$\mathbf{k}_0 = \boldsymbol{\varphi}(t^n, \mathbf{U}^n) \tag{58}$$

$$\mathbf{k}_1 = \boldsymbol{\varphi}(t^n + \frac{\triangle t}{2}, \mathbf{U}^n + \mathbf{k}_0 \frac{\triangle t}{2}) \tag{59}$$

$$\mathbf{k}_2 = \boldsymbol{\varphi}(t^n + \frac{\triangle t}{2}, \mathbf{U}^n + \mathbf{k}_1 \frac{\triangle t}{2}) \tag{60}$$

$$\mathbf{k}_3 = \boldsymbol{\varphi}(t^n + \triangle t, \mathbf{U}^n + \mathbf{k}_2 \triangle t) \tag{61}$$

To estimate the efficiency improvement, the computation times have been compared in several cases. We consider that convergence has been achieved when the increment of all the variables (h, hu, hv) is smaller than a certain tolerance ε. We usually take the tolerance value $\varepsilon = 10^{-6}$ when using the forward Euler method.

The time step Δt used with the Adams–Moulton method is about nine times bigger than the one used with the Euler method. For the Runge–Kutta method this ratio increases up to 25. This means that the variables change at every time step is much greater than the one from the Euler method. To properly compare the efficiency, the tolerance $k \times 10^{-6}$ in the conducted tests was used, k being the ratio between the time step of each one of the two methods and that of Euler's. In this way, when the process stops, the variation of the variables per unit time is approximately the same for the three methods.

For both methods the steady state is achieved in a much smaller number of iterations than using the Euler method. On the other hand, the computational time for one time step is greater in both methods than in Euler's: it was about four times greater using the Runge–Kutta method and two times using the Adams–Moulton method.

Next, two examples of the computational time saving are shown. Both have been calculated with a regular mesh of 41×41 nodes and for two different viscosities and upwinding coefficient values. The results obtained are

(1) $v = 0.01, c_d = 0.05$.

- Euler. Number of iterations: 12 965.
- Runge–Kutta. Number of iterations: 518.
- Adams–Moulton. Number of iterations: 1439.

The approximate computation time percentages are:

- Runge–Kutta/Euler: $\%T_c = \frac{518 \cdot 4}{12965} 100 = 15.98\%$.
- Adams–Moulton/Euler: $\%T_c = \frac{1439 \cdot 2}{12965} 100 = 22.20\%$.
- Runge–Kutta/Adams–Moulton: $\%T_c = \frac{518 \cdot 4}{1439 \cdot 2} 100 = 71.99\%$.

(2) $v = 0.0001, c_d = 0.06$.

- Euler. Number of iterations: 81 755.
- Runge–Kutta. Number of iterations: 2172.
- Adams–Moulton. Number of iterations: 6033.

The approximate computation time percentages are:

- Runge–Kutta/Euler: $\%T_c = \frac{2172 \cdot 4}{81755} 100 = 10.62\%$.
- Adams–Moulton/Euler: $\%T_c = \frac{6033 \cdot 2}{81755} 100 = 14.76\%$.
- Runge–Kutta/Adams–Moulton: $\%T_c = \frac{2172 \cdot 4}{6033 \cdot 2} 100 = 72.00\%$.

It can be noted that the computational savings with respect to Euler's, attained by using each method, are different: the ratios vary, in the two described cases, from 10.62 to 15.98% (Runge–Kutta/Euler) and from 14.76 to 22.20% (Adams–Moulton/Euler). However, the ratio of computation times between the two of them stays the same (72%, in favor of Runge–Kutta).

It is interesting to remark that this saving has been obtained when the numerical viscosity is reduced by the upwinding coefficient. If there is no reduction, then no computation time saving is achieved using the Runge–Kutta or the Adams–Moulton method. It may also be pointed out that the smaller the viscosity, the greater the efficiency improvement observed.

8. CONCLUSIONS

A first-order finite volume model for the resolution of the shallow water equations with turbulent term was presented, showing that the consideration of this term greatly improves the accuracy in the representation of 2D recirculating viscous flows. However, the numerical viscosity (or diffusion) produced by the upwinding of the flux term hinders the appreciation of the effect of using different viscosity values. It is thus important to diminish the numerical viscosity, which distorts the results, so that it does not interfere with the imposed viscosity. The use of a coefficient in the upwinding term has proved to effectively reduce this numerical viscosity.

In order to discretize the turbulent term, two methods were described and compared. It is shown that the method that uses gradient mean values gives better results than the one that makes use of directional derivatives.

Finally, the fourth-order Adams–Moulton and Runge–Kutta discretizations of the time derivative were tested and both of them were proved to be much more efficient than the forward Euler method, provided the numerical viscosity is reduced. Otherwise no improvement is achieved. The Runge–Kutta method has shown more efficiency than the Adams–Moulton method.

ACKNOWLEDGEMENTS

This work has been partially supported by Grant # PGIDIT06TAM11801PR and PGIDIT05PXIC 118002PN of the *Xunta de Galicia*, by Grant # DPI2004-05156, DPI2006-15275 and DPI2007-61214 of the *Ministerio de Educación y Ciencia* cofinanced with FEDER funds and by research fellowships of the *Universidad de A Coruña* and the *Fundación de la Ingeniería Civil de Galicia*.

REFERENCES

1. Vreugdenhil CB. *Numerical Methods for Shallow-water Flow*. Kluwer Academic Publishers: Dordrecht, The Netherlands, 1994.
2. Peraire J, Zienkiewicz OC, Morgan K. Shallow water problems: a general explicit formulation. *International Journal for Numerical Methods in Engineering* 1986; **22**:547–574.
3. Quecedo M, Pastor M. A reappraisal of Taylor–Galerkin algorithm for drying–wetting areas in shallow water computations. *International Journal for Numerical Methods in Fluids* 2002; **38**:515–531.
4. Ribeiro FLB, Galeao AC, Landau L. Edge-based finite element method for shallow water equations. *International Journal for Numerical Methods in Fluids* 2001; **36**:659–685.
5. Sheu TWH, Fang CC. High resolution finite-element analysis of shallow water equations in two dimensions. *Computer Methods in Applied Mechanics and Engineering* 2001; **190**:2581–2601.
6. Hauke G. A stabilized finite element method for the Saint Venant equations with application to irrigation. *International Journal for Numerical Methods in Fluids* 2002; **38**:963–984.

DOI: 10.1002/fld

7. Alcrudo F, García-Navarro P. A high resolution Godunov type scheme in finite volumes for the 2D shallow-water equations. *International Journal for Numerical Methods in Fluids* 1993; **16**:489–505.
8. Chippada S, Dawson CN, Martínez ML, Wheeler MF. A Godunov-type finite volume method for the system of shallow water equations. *Computer Methods in Applied Mechanics and Engineering* 1998; **151**:105–129.
9. Anastasiou A, Chan CT. Solution of the shallow water equations using the finite volume method on unstructured triangular meshes. *International Journal for Numerical Methods in Fluids* 1997; **24**:1225–1245.
10. Zhao DH, Shen HW, Tabios GQ, Lai JS, Tan WY. Finite-volume two-dimensional unsteady-flow for river basins. *Journal of Hydraulic Engineering* 1994; **120**:864–883.
11. Alcrudo F. A state of the art review on mathematical modelling of flood propagation. *Report of the Investigation of Extreme Flood Processes and Uncertainty* (*IMPACT*). Available from: www.samui.co.uk/impact-project/.
12. Cea L, French JR, Vázquez-Cendón ME. Numerical modelling of tidal flows in complex estuaries including turbulence: an unstructured finite volume solver and experimental validation. *International Journal for Numerical Methods in Engineering* 2006; **67**:1909–1932.
13. Bermúdez A, Dervieux A, Desideri J, Vázquez ME. Upwind schemes for the two dimensional shallow water equations with variable depth using unstructured meshes. *Computer Methods in Applied Mechanics and Engineering* 1998; **155**:49–72.
14. Mingham CG, Causon DM. High-resolution finite-volume method for shallow water flows. *Journal of Hydraulic Engineering* 1998; **124**(6):604–614.
15. Vázquez-Cendón ME. Improved treatment of source terms in upwind schemes for the shallow water equations in channels with irregular geometry. *Journal of Computational Physics* 1999; **148**:497–526.
16. Brufau P, García-Navarro P. Two-dimensional dam break flow simulation. *International Journal for Numerical Methods in Fluids* 2000; **33**:35–57.
17. Bradford S, Katopodes ND. Finite volume model for nonlevel basin irrigation. *Journal of Irrigation and Drainage Engineering* (ASCE) 2001; **127**(4):216–223.
18. Brocchini M, Bernetti R, Mancinelli A, Albertini G. An efficient solver for nearshore flows based on the WAF method. *Coastal Engineering* 2001; **43**:105–129.
19. Fe J. Aplicación del método de volúmenes finitos a la resolución numérica de las ecuaciones de aguas someras con incorporación de los esfuerzos debidos a la turbulencia. *Ph.D. Dissertation* (in Spanish), University of A Coruña, 2005. Available from: http://www.tesisenred.net/.
20. Falconer RA. A two-dimensional mathematical model study of the nitrate level in an natural inland basin. *Proceedings of the International Conference on Water Quality Modelling in the Inland Natural Environment*, BHRA Fluid Engineering, Bournemouth, 1986; 325–334.
21. Vellando P, Puertas J, Colominas I. SUPG stabilized finite element resolution of the Navier–Stokes equations. Applications to water treatment engineering. *Computer Methods in Applied Mechanics and Engineering* 2002; **191**:5899–5922.
22. Castanedo S, Medina R, Mendez FJ. Models for the turbulent diffusion terms of shallow water equations (technical note). *Journal of Hydraulic Engineering* 2005; **131**:217–222.
23. Harten A, Lax P, Van Leer B. On upstream differencing and Godunov-type schemes for hyperbolic conservation laws. *SIAM Review* 1983; **25**:35–61.
24. Burggraf OR. Analytical and numerical studies of the structure of steady separated flows. *Journal of Fluid Mechanics* 1966; **24**(1):113–152.
25. Ghia U, Ghia KN, Shin CT. High-Re solutions for incompressible flow using the Navier–Stokes equations and a multigrid methods. *Journal of Computational Physics* 1982; **48**:387–411.
26. Donea J, Huerta A. *Finite Element Methods for Flow Problems*. Wiley: Chichester, 2003.
27. Sahin M, Owens RG. A novel fully implicit finite volume method applied to the lid-driven cavity problem—Part I: high Reynolds number flow calculations. *International Journal for Numerical Methods in Fluids* 2003; **42**:52–77.
28. Bui T. A parallel, finite-volume algorithm for large-eddy simulation of turbulent flows. *NASA/TM-1999-206570*. Dryden Flight Research Center, Edwards, CA, 1999.
29. Lin S, Chen Y, Shih S. Numerical study of MUSCL schemes for computational aeroacoustics. *AIAA-97-0023*, January 1997.
30. Stoer J, Burlish R. *Introduction to Numerical Analysis*. Springer: New York, 1980.

DOI: 10.1002/fld